IEEE Access
Multidisciplinary ⋮ Rapid Review ⋮ Open Access Journal

Received 10 December 2022, accepted 18 January 2023, date of publication 23 January 2023, date of current version 26 January 2023.

Digital Object Identifier 10.1109/ACCESS.2023.3238996

RESEARCH ARTICLE

Theorizing a Simple Ferrite Cored Coil Using Image Coils in Wireless Power Transfer

YUTO YAMADA, (Graduate Student Member, IEEE), TAKEHIRO IMURA, (Member, IEEE), AND YOICHI HORI, (Life Fellow, IEEE)

Faculty of Engineering, Tokyo University of Science, Chiba 278-8510, Japan

Corresponding author: Yuto Yamada (yuto.yamada20@gmail.com)

ABSTRACT The technology of wireless power transfer, which wirelessly transmits power to any device, has been widely studied. Wireless power transfer using magnetic field resonance involves the use of coils and a material called ferrite, which improves the transmission characteristics. Until now, electromagnetic field analysis has been used to design ferrite cored coils, but electromagnetic field analysis requires a long analysis time and a computer with a large amount of memory. In this study, the ferrite shield and coil are represented as a image coil under the condition that the positional relationship between the ferrite shield and the coil does not change. This enabled the derivation of mutual inductance only by numerical analysis, which had been difficult up to now. In addition, experiments have shown that when the coil size does not change, mutual inductance can be derived only by numerical analysis using arbitrary coil parameters, regardless of the number of turns and pitch. The average error in deriving the design value was 5.2%. This facilitated the design of ferrite cored coils at 85 kHz and contributed greatly to the design of the system.

INDEX TERMS Wireless power transfer, ferrite core, coil design, numerical analysis, inductive wireless power transfer, image method.

I. INTRODUCTION

Wireless power transfer is a technology for transmitting power wirelessly to all kinds of devices. Since power can be transmitted without cables, it has been actively researched in recent years from the viewpoints of expected convenience, utilization of devices in new environments [1], and durability of cables against abrasion, etc. The challenges imposed on wireless power transfer include lower transmission power due to the wireless connection, lower transmission efficiency, adverse effects such as noise on neighboring devices, and harmful effects on the surrounding human body, and there are regulatory values for magnetic field strength [2], [3], [4], [5]. In wireless power transfer using magnetic field resonance, a widely recognized means of solving these problems is to attach a core called a ferrite in the coil. This allows the magnetic field generated by the coil to be organized and suppresses unnecessary spreading, which is expected to improve inductance and lower magnetic field leakage. However, the design of coils with ferrite core has so far been based on electromagnetic field analysis because it is difficult to capture the phenomenon. Electromagnetic field analysis can represent the power transmission environment very accurately, but it has the problem of requiring a lot of PC memory and analysis time [6]. And it requires expensive analysis software. The actual design parameters for wireless power transfer include not only coil size, number of turns, pitch and transmission distance, but also the input voltage of the circuit, loading conditions, circuit system and many other factors, making it difficult to perform parametric analysis of many parameters using electromagnetic field analysis. Therefore, it is very significant to design various parameters simultaneously at high speed by numerical analysis. It is also very important to express and think theoretically in terms of design.

In references [7], [8], [9], [10], [11], and [12], the high permeability material such as ferrite attached in the coil is represented by a image coil, which exists in a plane symmetrical to the ferrite boundary plane. In reality, however, the ferrite shield is of finite size and thickness, which introduces errors in the design values. In [13], the concept of a virtual

The associate editor coordinating the review of this manuscript and approving it for publication was Diego Masotti.

mirror image plane is introduced to correct the position of the image coil under realistic conditions. Furthermore, it is shown that the position of the virtual mirror image plane does not change when the coil size does not change. However, there is an issue that the representation of the image coil into the equivalent circuit is different in magnetic materials. In addition, although it states that the position of the virtual mirror image plane does not change when the coil size does not change, the shape change in the number of turns and pitch is not large, and there are questions about the design in the case of even larger changes. Reference [14] similarly replaces coil design with electromagnetic field analysis, but it requires an algorithm.

In this study, in order to design a ferrite cored coil in a more realistic situation, the method of determining the virtual mirror image plane is presented, and it is verified by producing several coils that the position of the virtual mirror image plane does not change. In Chapter II, the method of representing the ferrite shield in the image coil is explained, in Chapter III, the design method of the ferrite cored coil and comparison with experimental values are shown, and in Chapter IV, the conclusion is presented.

II. EXPRESSION OF FERRITE CORES IN IMAGE COILS

The self-inductance and mutual inductance of a coil greatly affect the characteristics of wireless power transfer, so appropriate design is necessary. While the installation of a ferrite core in a coil improves the characteristics of the coil, it also makes it difficult to design the coil by numerical analysis. Here, a ferrite-cored coil is represented by a coreless coil and image coils, and the self-inductance and mutual inductance are derived by numerical analysis, assuming that only an coreless coil exists in the space.

A. DERIVATION OF SELF-INDUCTANCE L AND MUTUAL INDUCTANCE L_m OF CORELESS COIL

In deriving the self and mutual inductance of a ferrite cored coil, it is necessary to derive the self and mutual inductance at the coreless coils. The respective derivation methods are described below.

1) DERIVATION OF THE SELF-INDUCTANCE L OF THE COIL

Accurate derivation of self-inductance is very important to characterize the circuit and to set the appropriate resonant capacitor. (1) is the formula for the derivation of the self-inductance L of a square spiral coil [15], where d_a is the diameter of the Litz wire conductor and α is the length of the gap between the Litz wires, expressed as $\alpha = p - d_a$. The parameters used to derive the self-inductance are shown in FIGURE 1. Pitch p, the distance between Litz wires, is shown in FIGURE 2.

$$L = 0.635\mu d_{ave} N^2 \left\{ \ln\left(\frac{2.07}{\rho}\right) + 0.18\rho + 0.13\rho^2 \right\} \tag{1}$$

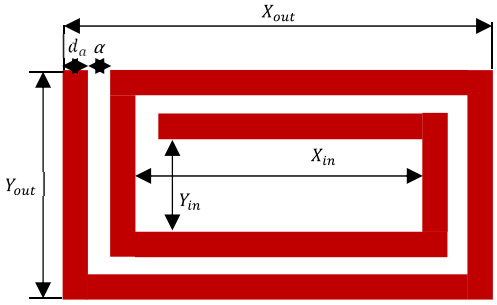

FIGURE 1. Coil parameters used to derive self-inductance.

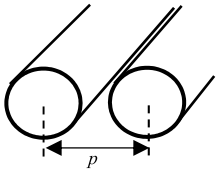

FIGURE 2. Pitch (Distance between wire to wire).

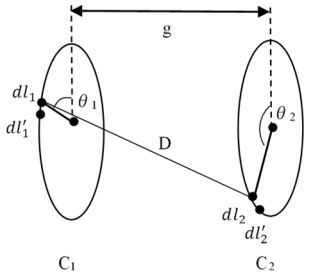

FIGURE 3. Parameters of the Neumann equation.

$$d_{ave} = \frac{1}{4}(X_{in} + X_{out} + Y_{in} + Y_{out}) \tag{2}$$

$$\rho = \frac{1}{2}\left(\frac{X_{out} - X_{in}}{X_{out} + X_{in}} + \frac{Y_{out} - Y_{in}}{Y_{out} + Y_{in}}\right) \tag{3}$$

2) DERIVATION OF THE MUTUAL-INDUCTANCE L_m OF THE COIL

During wireless power transfer, coupling occurs between the primary and secondary coils, the proportion of which is expressed by the coupling coefficient k. Together with the coupling coefficient and the self-inductance, the mutual inductance can be obtained, which is a very important parameter in circuit calculations. The equation that can directly express the mutual inductance is called the Neumann equation and can be expressed as (4) [16]. The parameters used in (4) are shown in FIGURE 3.

$$L_m = \frac{\mu_0}{4\pi} \oint_{C1} \oint_{C2} \frac{dl_1 dl_2}{D} \tag{4}$$

B. DERIVATION OF SELF AND MUTUAL INDUCTANCE WHEN FERRITE IS ATTACHED

The mirror image method is used as a simple method to capture the spatial distribution of electric and magnetic fields in a

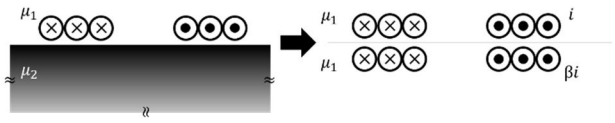

FIGURE 4. Ideal semi-infinite space and location of image coil.

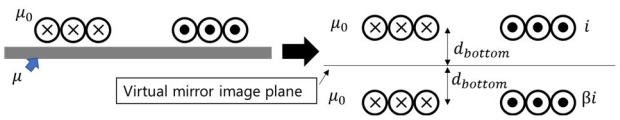

FIGURE 5. Location of image coils when ferrite is attached.

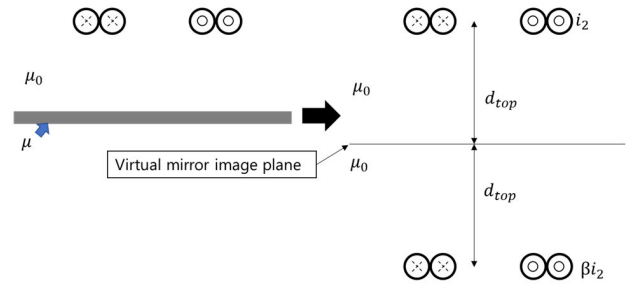

FIGURE 6. Location of image coil by opposite ferrite.

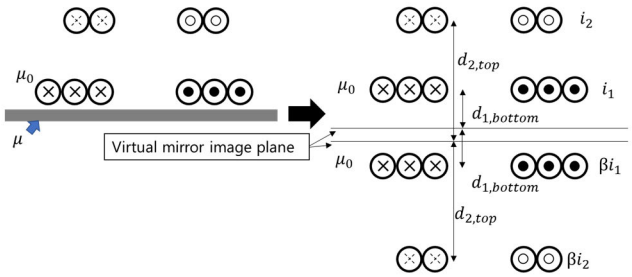

FIGURE 7. Expression by image coil when ferrite is attached on one side.

space where materials with different dielectric constants and magnetic permeability exist. If the semi-infinite spaces with permeabilities μ_1 and μ_2 are bounded as in FIGURE 4 and there exists a coil through which the current i flows, the transformation can be done as in FIGURE 4 using the image coil. The current flowing in the image coil can be expressed by (5) using the permeability distributed in the space. Although ferrite is a material with high permeability, it is not possible to set the image coil in a position symmetrical to the boundary plane due to size and thickness limitations compared to the ideal situation as shown in FIGURE 4. Therefore, a virtual boundary surface is set as shown in FIGURE 5, and it is referred to as a virtual mirror image surface. The distance from the virtual mirror image plane due to the ferrite itself is expressed as d_{bottom}.

Inductance of the standard coil and position of the virtual mirror image plane obtained by electromagnetic field analysis.

$$\beta = \frac{\mu_2 - \mu_1}{\mu_2 + \mu_1} \tag{5}$$

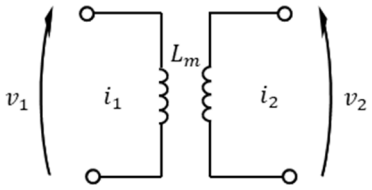

FIGURE 8. Circuit used to explain circuit equations.

1) DERIVATION OF THE SELF INDUCTANCE L_f OF THE FERRITE CORED COIL

The ferrite cored coil L_{1f} has a main coil L_{1a} and a image coil $L_{11'}$ with the same inductance as the main coil, as shown in FIGURE 5. When current i flows in the main coil L_{1a}, current βi also flows in the image coil $L_{11'}$. The ferrite cored coil can be considered that the magnetic flux from the image coil $L_{11'}$ also flows into the main coil L_{1a}. Therefore, the self-inductance L_{1f} can be expressed by (6) using the mutual inductance $M_{11'}$ between the main coil L_{1a} and the image coil $L_{11'}$. The procedure for deriving the distance d_{bottom} to the virtual mirror image plane is shown below.

Step1: Derive the self-inductance of the ferrite cored coil L_{1f} by electromagnetic field analysis.

Step2: Derive the self-inductance of the coreless coil L_{1a} with the ferrite removed.

Step3: Calculate the mutual inductance between the coreless coils L_{1a} and find the distance d_{bottom} to the virtual mirror image plane that satisfies (6).

By determining the distance to the virtual mirror image plane, the number of turns and pitch can be freely designed, as long as the coil size does not change [12]. The fact that design is possible using the same virtual mirror image surface is explained in Chapter 3 through actual measurements.

$$L_{1f} = L_{1a} + \beta M_{11'} \tag{6}$$

2) DERIVATION OF THE MUTUAL INDUCTANCE L_m OF THE FERRITE CORED COIL

Consider the power transmission condition where a ferrite is attached in one of the coils. In this case, the ferrite can be considered to be attached at a distance from the coreless coil, so a virtual mirror image plane is set as shown in FIGURE 6, and the distance d_{top} to the virtual mirror image plane by the ferrite relative to the other coil is set. The method for obtaining the distance d_{top} is the same as in B.1). The positional relationship between the image coil $L_{1'}$ of the primary coil and the image coil $L_{2''}$ of the secondary coil is summarized as in FIGURE 7.

From FIGURE 5 and FIGURE 6 and the relationship in (6), the position of each image coil on the primary and secondary sides can be determined.

Now that the positions of all the image coils have been determined, the derivation of the mutual inductance L_m when a ferrite is attached on one side is explained. Equations (7) and (8) are circuit equations for the circuit shown in FIGURE 8. Equation (7) is represented by the self-inductance L_{1a} of the coreless coil of the primary coil, mutual inductance $M_{11'}$ of the primary coil with the image coil by its own ferrite, the mutual inductance M_{12} considering the magnetic flux flowing into the primary coil L_{1a} from the secondary coil L_{2a}, the mutual inductance $M_{12''}$ considering the magnetic flux flowing into the primary coil L_{1a}

For M_{12} and M_{21}, the reciprocity theorem holds because they are coreless to coreless, but for (9) and (10), the reciprocity theorem for mutual inductance does not hold because image coils are used. However, since no difference in mutual inductance appears in actual wireless power transfer, the mutual inductance of the ferrite cored coil is expressed by (11).

$$v_1 = j\omega\left(L_{1a} + \beta M_{11'}\right) i_1 + j\omega(M_{12} + \beta M_{12''}) i_2 \tag{7}$$

$$v_2 = j\omega\left(M_{21} + \beta M_{21'}\right) i_1 + j\omega(L_{2a} + \beta M_{22''}) i_2 \tag{8}$$

$$L_{m,12} = M_{12} + \beta M_{12''} \tag{9}$$

$$L_{m,21} = M_{21} + \beta M_{21'} \tag{10}$$

$$L_m = \frac{L_{m,12} + L_{m,21}}{2} \tag{11}$$

C. DERIVATION OF MUTUAL INDUCTANCE L_m WHEN FERRITE IS ATTACHED ON BOTH PRIMARY AND SECONDARY SIDE

In this section, the power transmission environment in which ferrites are attached to both the primary and secondary side is considered, as in FIGURE 9. As explained in B.2), it is necessary to consider not only the image coils the image coils of the ferrites on the opposite sides. Furthermore, when ferrites are sandwiched between each other, image coils are continuously generated against the image coils.

Equation (12) and (13) represent the position of the image coil [8]. $Z'_{i,k}$ represents the coordinates of successive image coils on its own ferrite side and $Z''_{i,k}$ represents the coordinates of successive image coils on the side opposite its ferrite. i represents the primary or secondary side ($i = 1$ or 2) and k represents the level of the image coil. FIGURE 9 shows four types of image coils with up to 1st level, both primary and secondary. Although there are many successive level of image coils, it is sufficient to derive the mutual inductance up to 5th level [8]. Equation (14) shows the current $i_{i,k}$ flowing in each of the primary and secondary in the k th level of image coils.

$$Z'_{i,k} = 2\left\{\left[\frac{k+1}{2}\right] d_i, bottom - \left[\frac{k}{2}\right] d_i, top\right\} \tag{12}$$

$$Z''_{i,k} = 2\left\{\left[\frac{k+1}{2}\right] d_i, top - \left[\frac{k}{2}\right] d_i, bottom\right\} \tag{13}$$

$$i_{i,k} = \beta^k i_i \tag{14}$$

Next, the representation on the equivalent circuit when multiple image coils are present is shown. Again, when considering the equivalent circuit of FIGURE 8, the circuit equations can be expressed as (15) and (16). For example, $M_{12'_k}$ represents the mutual inductance between the primary coreless coil L_{1a} and the kth level of image coil on the bottom side of the secondary. $M_{21''_k}$ represents the mutual inductance between the secondary side coreless coil L_{2a} and the kth level of image coil on the top side of the primary.

From (15) and (16), the mutual inductance from the primary side and the secondary side are shown in (17) and (18), respectively. From this, the mutual inductance of the entire circuit can be expressed by (19). The positions of the image coils are obtained in (12) and (13), and can be easily derived by numerical analysis in (4), since they are replaced with each other by coreless coils. In other words, if the distance d_{1_bottom}, d_{1_top}, d_{2_bottom}, d_{2_top} to the virtual mirror plane can be obtained by electromagnetic field analysis once with the standard coil when the coil size, distance between the ferrite and the coil, and the ferrite size and transmission distance remain unchanged, it can be seen that the self-inductance and mutual inductance of a ferrite cored coil can be derived using only an coreless coil.

$$v_1 = j\omega\left\{L_{1a} + \sum_{k=1}^{5}\left(\beta^k M_{11'_k} + \beta^k M_{11''_k}\right)\right\} i_1 + j\omega\left\{M_{12} + \sum_{k=1}^{5}\left(\beta^k M_{12'_k} + \beta^k M_{12''_k}\right)\right\} i_2 \tag{15}$$

$$v_2 = j\omega\left\{M_{21} + \sum_{k=1}^{5}\left(\beta^k M_{21'_k} + \beta^k M_{21''_k}\right)\right\} i_1 + j\omega\left\{L_{2a} + \sum_{k=1}^{5}\left(\beta^k M_{22'_k} + \beta^k M_{22''_k}\right)\right\} i_2 \tag{16}$$

$$L_{m,12} = M_{12} + \sum_{k=1}^{5}\left(\beta^k M_{12'_k} + \beta^k M_{12''_k}\right) \tag{17}$$

$$L_{m,21} = M_{21} + \sum_{k=1}^{5}\left(\beta^k M_{21'_k} + \beta^k M_{21''_k}\right) \tag{18}$$

$$L_m = \frac{L_{m,12} + L_{m,21}}{2} \tag{19}$$

III. DESIGN PROCEDURES AND EXPERIMENTAL VALIDATION

In this chapter, the design method for coils with ferrites attached on both the primary and secondary sides is described according to the procedure, and the experimental and

TABLE 1. Parameters of standard coil.

	Primary Side	Secondary Side
Number of turns	10	14
Pitch p [mm]	3.4	3.4
Size of Coil [mm]	350×250	250×250
Ferrite	TDK PC95	TDK PC95
Size of ferrite [mm]	400×300	400×300
Distance between coil and ferrite [mm]	3	3
Thickness of ferrite [mm]	5	5

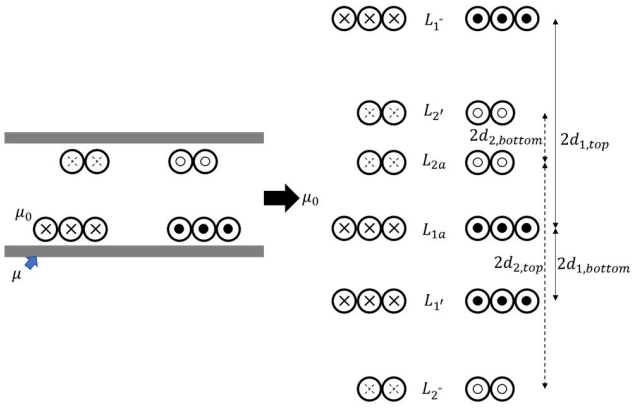

FIGURE 9. Location of image coils when sandwiched by ferrite (up to the first level).

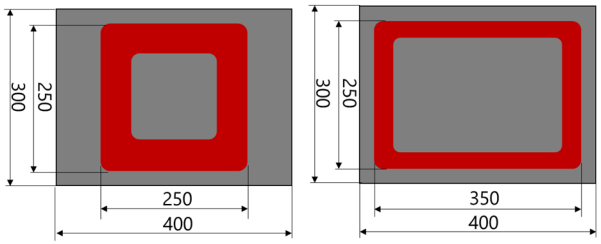

FIGURE 10. Coil size of standard coil.

theoretical values are compared. The goal is to optimize the coils, but since optimization can be done freely by showing how to derive self-inductance and mutual inductance, the goal of this paper is to achieve agreement between experimental and theoretical values.

A. SETUP OF POWER TRANSMISSION ENVIRONMENT

In order to represent a ferrite cored coil as a image coil and to derive it only by numerical analysis, it is necessary to set up a standard coil and determine the size and thickness of the ferrite, the distance between the ferrite and the coil, and the transmission distance.

Assuming power transmission frequency at 85 kHz, a Litz wire with 500 strands and a strand diameter of 0.1 mm was used. The transmission distance was set at 103 mm. Table 1 summarizes the standard coil. FIGURE 10 and FIGURE 11 shows the standard coil size and power transmission environment.

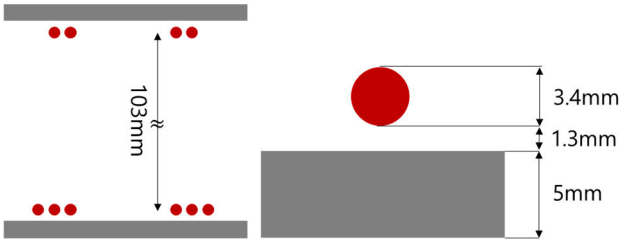

FIGURE 11. Location of coil and ferrite.

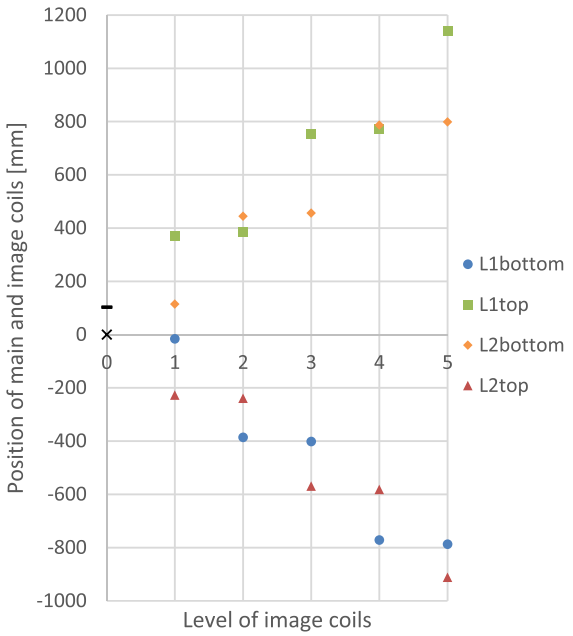

FIGURE 12. Coordinates of image coils and main coils up to the 5th level.

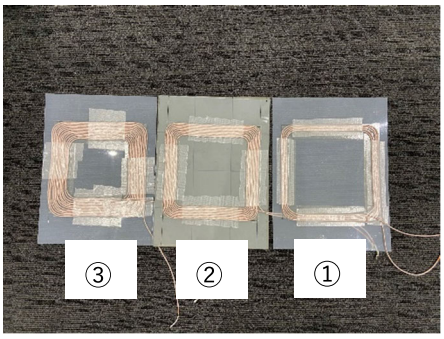

FIGURE 13. Produced secondary side coil.

B. DETARMINE THE VIRTUAL MIRROR IMAGE PLANE OF THE STANDARD COIL

In this section, the virtual mirror image plane of the standard coil is obtained from (9) and (10), and the coordinates of the image coil up to the 5th level are obtained from (12) and (13).

The initial permeability of PC95 used is 3300, which is much larger than 1. Therefore, since the current decrease rate β of the image coil is almost 1, the effect of β is neglected here. Table 2 shows the inductance of the standard coil obtained by electromagnetic field analysis and the position of the virtual mirror plane of the image coil. Since the transmission distance this time is 103 mm, the coordinates of

TABLE 2. Inductance of the standard coil and position of the virtual mirror image plane obtained by electromagnetic field analysis.

	Primary	Secondary
Inductance L_{ia} [μH]	57.8	69.7
Inductance L_{if} [μH]	98.1	125.2
Distance d_{i_bottom} [mm]	-15.5	12.0
Distance d_{i_top} [mm]	370.0	-370.0

TABLE 3. Number of turns and pitch of secondary coil.

Coil Number	Turns	Pitch p [mm]
①	5	3.4
②	10	3.4
③	14	3.4

TABLE 4. Number of turns and pitch of primary coil.

Coil Number	Turns	Pitch p [mm]
④	5	3.4
⑤	10	3.4
⑥	15	3.4
⑦	20	3.4
⑧	25	3.4
⑨	5	6.8
⑩	10	6.8
⑪	13	6.8

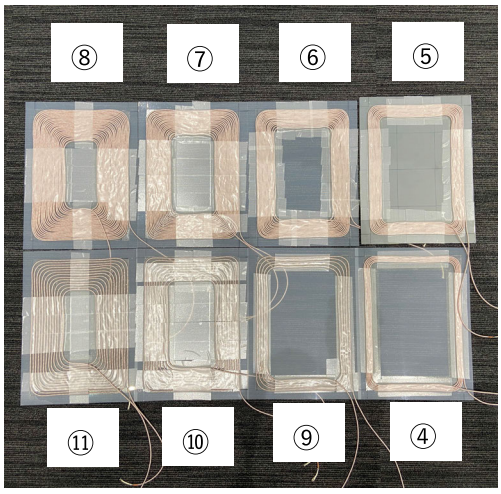

FIGURE 14. Produced primary side coil.

the image coil are obtained by adding 103 mm to d_{2_bottom} and d_{2_top} on the secondary side.

The coordinates of the primary coil are 0 mm and the coordinates of the secondary coil are 103 mm. FIGURE 12 shows the coordinates of each image level of the image coils up to the 5th stage. As the distance from the main coil increases with the number of levels, the magnetic flux flowing into the main coil decreases, and the mutual inductance obtained from (17) and (18) is expected to converge. The location where the level is 0 indicates the original main coil coordinates.

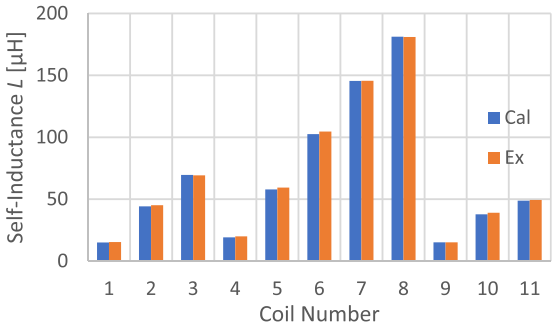

FIGURE 15. Comparison of calculated and experimental values of self-inductance.

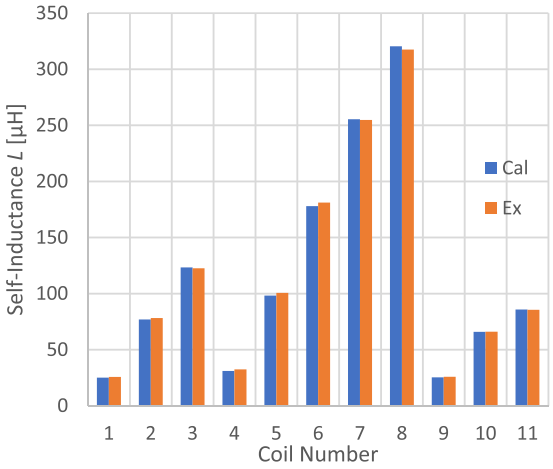

FIGURE 16. Comparison of calculated and experimental values of self-inductance.

C. DERIVATION OF SELF AND MUTUALINDUCTANCE OF VARIOUS COILS

In this section, several coils with the same size as the standard coil and with different numbers of turns and pitches are produced, and the inductance of the theoretically obtained by using the image coil obtained in section III-B is compared with the experimental value.

Table 3 and Table 4 summarizes the coils produced this time. The coils produced are shown in FIGURE 13 and FIGURE 14.

1) DERIVATION OF THE SELF-INDUCTANCE L OF THE FERRITE CORED COIL

Since the produced coil has the same distance relationship to the virtual mirror image plane as the standard coil for both the primary and secondary sides, the self-inductance can be obtained both with and without the ferrite in (1), (4) and (6)

Calculated and experimented values were compared with FIGURE 15and FIGURE 16 along the coil numbers listed in Table 3 and Table 4. The calculated and experimental values agreed very well.

2) DERIVATION OF THE MUTUAL INDUCTANCE L_m OF THE FERRITE CORED COIL

Since all the produced coils have the same distance relationship to the virtual mirror image plane as the standard coil, the

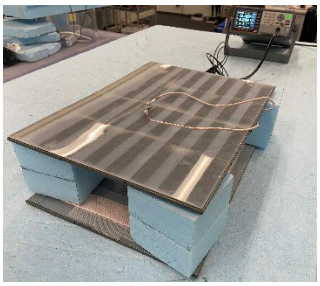

FIGURE 17. Measurement scenery.

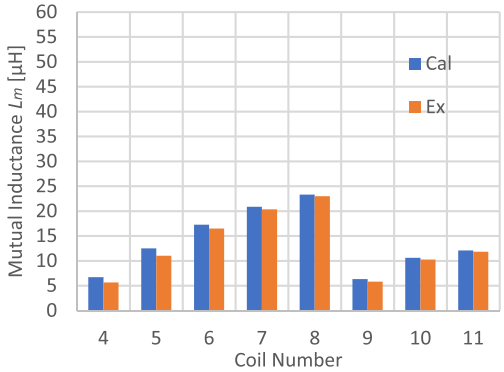

FIGURE 18. Mutual inductance of the primary coil relative to the number coil of the ferrite cored coil.

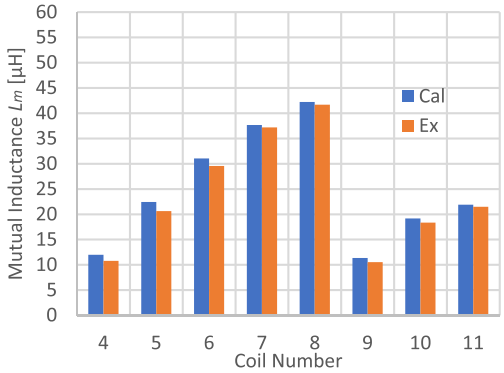

FIGURE 19. Mutual inductance of the primary coil relative to the number ② coil of the ferrite cored coil.

mutual inductance of the ferrite cored coils can be obtained from (4) and (19) as in C.1). The measurement scene is shown in FIGURE 17. FIGURE 18 shows the mutual inductance of the ferrite cored coils of primary coils (number 4 to 11) for the coil with secondary coil number 1. Due to the small self-inductance, the average error rate was 7.0%. FIGURE 19 shows the mutual inductance of the ferrite cored coils of primary coils (number 4 to 11) for the coil with secondary coil number 2. The average error rate was kept at 5.2%. FIGURE 20 shows the mutual inductance of the ferrite cored coils of primary coils (number 4 to 11) for the coil with secondary coil number 3. The large self-inductance allowed us to reduce the average error rate to 3.5%. It can be seen that the calculated and experimental values are in good agreement for any combination of coils.

FIGURE 21 shows how the mutual inductance due to the image coils obtained by the calculated values increases with each additional level of the image coils. Coil numbers 2

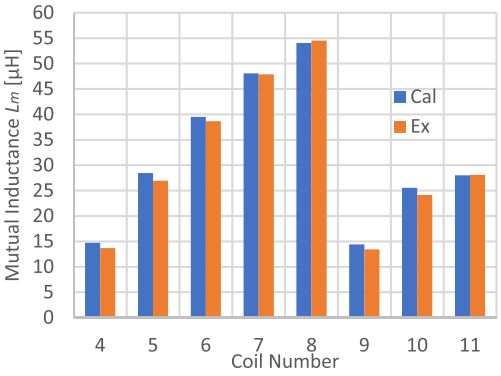

FIGURE 20. Mutual inductance of the primary coil relative to the number ③ coil of the ferrite cored coil.

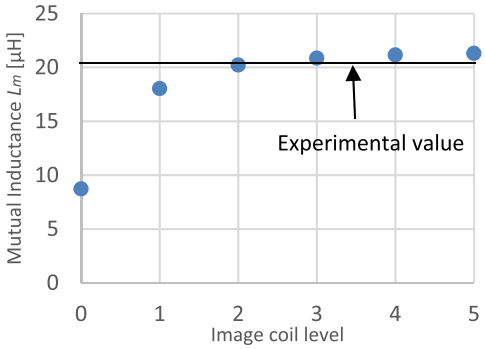

FIGURE 21. Mutual inductance of image coils at each level.

and 5 are used and the mutual inductance results shown in (18). As mentioned in section III-B, it can be seen that the mutual inductance converges to the mutual inductance obtained by the experiment as the number of steps increases, indicating that the calculation up to the 5th level is sufficient. Consequently, by obtaining the virtual mirror image plane of the standard coil, the self and mutual inductances could be accurately obtained only by numerical analysis when the coil size, ferrite size, coil and ferrite arrangement, and transmission distance remain the same.

IV. CONCLUSION

In this study, the ferrite-cored coil is expressed as only coreless coil by the theoretical equation derived from the circuit equation by the image coil and the equivalent circuit.

This method enables us to derive the self-inductance and mutual inductance with high accuracy only by numerical analysis. The proposed theory was confirmed by experiments to be in good agreement. The accuracy of the mutual inductance derivation was 5.2% on average for the data presented in this study. However, it is difficult to describe magnetic materials in a simple way, and the challenge is that conditions such as the ferrite being placed far away from the air in which the coil exists, or the ferrite being small, or the ferrite being thin, lead to significant deviations from the ideal situation as in FIGURE 4, and may not be well described by numerical analysis alone. Also, if the position is misaligned, the secondary ferrite will no longer exist directly above the primary coil, and the position of the virtual mirror image plane may be misaligned or distorted. As described above, the proposed

method for deriving the virtual mirror image plane and the self and mutual inductances is not yet highly versatile, but it can be used to obtain a higher degree of freedom in coil design through numerical analysis alone, since the number of turns and pitch can be changed within a fixed coil size.

Since the analysis time by electromagnetic field analysis is very long in the case of ferrite coils, it is very important to derive a low cost by numerical analysis in order to consider various design parameters of the circuit. This study will generate new research themes, and it is expected that research on wireless power transfer will become more and more active.

REFERENCES

[1] A. Mahesh, B. Chokkalingam, and L. Mihet-Popa, "Inductive wireless power transfer charging for electric vehicles—A review," *IEEE Access*, vol. 9, pp. 137667–137713, 2021, doi: 10.1109/ACCESS.2021.3116678.
[2] *CiSPR 11 Consolidated Version*, IEC International Electrotechinical Commission, Geneva, Switzerland, Jan. 2019.
[3] International commission on Non-Ionizing Radiation Protection, "Guidelines for limiting exposure to time-varying electric, magnetic, and electromagnetic fields(up to 300 GHz)(1 Hz To 100 kHz)," *Health Phys.*, vol. 99, pp. 818–836, Jan. 2010.
[4] *Wireless Power Transfer for Light-Duty Plug-in/Electric Vehicles and Alignment Methodology J2954*, SAE International, USA, 2020. [Online]. Available: https://www.sae.org/
[5] F. Wen and X. Huang, "Human exposure to electromagnetic fields from parallel wireless power transfer systems," *Int. J. Environ. Res. Public Health*, vol. 14, no. 2, p. 157, 2017, doi: 10.3390/ijerph14020157.
[6] F. Wen and X. Huang, "Optimal magnetic field shielding method by metallic sheets in wireless power transfer system," *Energies*, vol. 9, no. 9, p. 733, Sep. 2016, doi: 10.3390/en9090733.
[7] J. Turowski and M. Turowski, *Engineering Electrodynamics: Electric Machine, Transformer, and Power Equipment Design*. Boston, MA, USA, 2017, sec. 5. [Online]. Available: https://www.taylorfrancis.com/books/mono/10.1201/b16373/engineering-electrodynamics-janusz-turowski-marek-turowski
[8] A. Juhas, N. Pekaric-Nadj, and H. Toepfer, "Magnetic field of rectangular current loop with sides parallel and perpendicular to the surface of high-permeability material," *Serbian J. Electr. Eng.*, vol. 11, no. 4, pp. 701–717, 2014.
[9] D. M. Beams and S. G. Annam, "Calculation of mutual inductance from magnetic vector potential for wireless power transfer applications," in *Proc. 44th Southeastern Symp. Syst. Theory (SSST)*, Mar. 2012, pp. 209–213, doi: 10.1109/SSST.2012.6195124.
[10] W. A. Roshen, "Analysis of planar sandwich inductors by current images," *IEEE Trans. Magn.*, vol. 26, no. 5, pp. 2880–2887, Sep. 1990, doi: 10.1109/20.104901.
[11] W. A. Roshen and D. E. Turcotte, "Planar inductors on magnetic substrates," *IEEE Trans. Magn.*, vol. 24, no. 6, pp. 3213–3216, Nov. 1988, doi: 10.1109/20.92379.
[12] W. Y. Lee, J. Huh, S. Y. Choi, X. V. Thai, J. H. Kim, E. A. Al-Ammar, M. A. El-Kady, and C. T. Rim, "Finite-width magnetic mirror models of mono and dual coils for wireless electric vehicles," in *IEEE Trans. Power Electron.*, vol. 28, no. 3, pp. 1413–1428, Mar. 2013, doi: 10.1109/TPEL.2012.2206404.
[13] Y. Yazaki, T. Imura, and H. Fujimoto, "Coil design method considering with required specification for 85 kHz wireless power transfer system," IEICT, Tech. Rep., 2018. [Online]. Available: https://ken.ieice.org/ken/paper/2018100471gU/
[14] A. Delgado, G. Di Capua, K. Stoyka, L. Shi, N. Femia, A. Maffucci, S. Ventre, P. Alou, J. A. Oliver, and J. A. Cobos, "Self and mutual inductance behavioral modeling of square-shaped IPT coils with air gap and ferrite core plates," *IEEE Access*, vol. 10, pp. 7476–7488, 2022, doi: 10.1109/ACCESS.2021.3138239.
[15] S. S. Mohan, M. del Mar Hershenson, S. P. Boyd, and T. H. Lee, "Simple accurate expressions for planar spiral inductances," *IEEE J. Solid-State Circuits*, vol. 34, no. 10, pp. 1419–1424, Oct. 1999, doi: 10.1109/4.792620.
[16] Y. Yamada and T. Imura, "An efficiency optimization method of static wireless power transfer coreless coils for electric vehicles in the 85 kHz band using numerical analysis," *IEEJ Trans. Electr. Electron. Eng.*, vol. 17, no. 10, pp. 1506–1516, Oct. 2022.

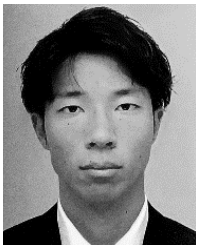

YUTO YAMADA (Graduate Student Member, IEEE) received the degree from the Department of Electrical Engineering, Faculty of Science and Technology, Tokyo University of Science, in March 2021. He is currently pursuing the degree with the Department of Electrical Engineering, Graduate School of Science and Technology, Tokyo University of Science. His current research interests include design of coils and circuit for wireless power transfer to electric vehicles and the realization of dynamic wireless power transfer. He is a Student Member of the Institute of Electrical Engineers of Japan (IEEJ).

TAKEHIRO IMURA (Member, IEEE) received the bachelor's degree in electrical and electronics engineering from Sophia University, Tokyo, Japan, in 2005, and the M.E. degree in electronic engineering and the D.Eng. degree in electrical engineering from The University of Tokyo, Tokyo, in 2007 and 2010, respectively. He joined the Department of Advanced Energy, Graduate School of Frontier Sciences, The University of Tokyo, as a Research Associate, where he has been a Project Lecturer, since 2015. In 2019, he joined the Department of Electrical Engineering, Tokyo University of Science, as an Associate Professor. He is currently investigating wireless power transfer using magnetic resonant coupling and electric resonant coupling. His research interests include electric vehicle in-motion connected to renewable energy, sensors, and cancer treatment. He is a member of the Institute of Electronics, Information and Communication Engineers (IEICE) and the Society of Automotive Engineers of Japan (JSAE). He is the Winner of the IEEJ Industry Applications Society Distinguished Transaction Paper Award, in 2015, and the IEEE Power Electronics Transactions First Prize Paper Award, in 2017.

YOICHI HORI (Life Fellow, IEEE) received the B.S., M.S., and Ph.D. degrees in electrical engineering from The University of Tokyo, Tokyo, Japan, in 1978, 1980, and 1983, respectively. In 1983, he joined the Department of Electrical Engineering, The University of Tokyo, as a Research Associate. Later, he became an Assistant Professor, an Associate Professor, and a Professor at The University of Tokyo, in 2000. In 2002, he moved to the Information and System Division, Institute of Industrial Science, as a Professor. In 2008, he moved to the Department of Advanced Energy, Graduate School of Frontier Sciences, The University of Tokyo. He retired in March 2021 and has been with the Tokyo University of Science, since April 2021. He was a Professor Emeritus with The University of Tokyo. From 1991 to 1992, he was a Visiting Researcher at the University of California at Berkeley. Recently, he has also been focusing on the research and promotion of wireless power transfer. His research interests include control theory and its industrial applications to motion control, mechatronics, robotics, and electric vehicles. He is a Past AdCom Member of Industrial Electronics Society (IES). He is currently a Fellow Member of the Institute of Electrical Engineers of Japan (IEEJ), the Society of Automotive Engineers of Japan (JSAE), and the Japan Society of Simulation Technology (JSST). He is the Winner of the Best Transactions Paper Award from the IEEE TRANSACTIONS ON INDUSTRIAL ELECTRONICS, in 1993, 2001, and 2013; the 2000 Best Transactions Paper Award from IEEJ; and the 2011 Achievement Award of IEEJ. He was the President of the Industry Applications Society of IEEJ and World Electric Vehicle Association (WEVA). He was the Director of the Japan Automobile Research Institute (JARI) and the Vice-President of JSAE. He is the President of Capacitors Forum, the Chairperson of the Motor Technology Symposium of Japan Management Association (JMA), and the Representative Director of the Next Generation Vehicle Promotion Center (NeV). He has been the Treasurer of the IEEE Japan Council and Tokyo Section in a few years, since 2001.